Development of cortical microstructure in the preterm human brain

Gareth Ball[a,1], Latha Srinivasan[b,1], Paul Aljabar[a,2], Serena J. Counsell[a], Giuliana Durighel[b], Joseph V. Hajnal[a], Mary A. Rutherford[a], and A. David Edwards[a,c]

[a]Centre for the Developing Brain, St. Thomas' Hospital, King's College London, London, SE1 7EH, United Kingdom; [b]Institute of Clinical Sciences, Hammersmith Hospital, Imperial College London, London W12 0HS, United Kingdom; and [c]Department of Bioengineering, Imperial College London, London SW7 2AZ, United Kingdom

Cortical maturation was studied in 65 infants between 27 and 46 wk postconception using structural and diffusion magnetic resonance imaging. Alterations in neural structure and complexity were inferred from changes in mean diffusivity and fractional anisotropy, analyzed by sampling regions of interest and also by a unique whole-cortex mapping approach. Mean diffusivity was higher in gyri than sulci and in frontal compared with occipital lobes, decreasing consistently throughout the study period. Fractional anisotropy declined until 38 wk, with initial values and rates of change higher in gyri, frontal and temporal poles, and parietal cortex; and lower in sulcal, perirolandic, and medial occipital cortex. Neuroanatomical studies and experimental diffusion–anatomic correlations strongly suggested the interpretation that cellular and synaptic complexity and density increased steadily throughout the period, whereas elongation and branching of dendrites orthogonal to cortical columns was later and faster in higher-order association cortex, proceeding rapidly before becoming undetectable after 38 wk. The rate of microstructural maturation correlated locally with cortical growth, and predicted higher neurodevelopmental test scores at 2 y of age. Cortical microstructural development was reduced in a dose-dependent fashion by longer premature exposure to the extrauterine environment, and preterm infants at term-corrected age possessed less mature cortex than term-born infants. The results are compatible with predictions of the tension theory of cortical growth and show that rapidly developing cortical microstructure is vulnerable to the effects of premature birth, suggesting a mechanism for the adverse effects of preterm delivery on cognitive function.

brain development | DTI | preterm birth

Dendritic arborization and synapse formation increase within the cerebral cortical plate from midgestation, transforming the cortex from a predominantly radial formation arrayed perpendicular to the cortical surface into a denser, more complex structure with large numbers of neural connections running parallel to the surface (1). Several groups have related this microstructural maturation to changes in the rate and principal direction of water diffusion within the cortex observed in vivo by diffusion tensor imaging (DTI) (2–5). It is proposed that increasing cellular density and complexity lead to a decrease in tissue water content and a fall in mean diffusivity (MD) (6–9), whereas decreases in the relative fraction of water diffusion perpendicular to the cortical surface, measured as a decline in fractional anisotropy (FA), reflect neurite outgrowth and maturing dendritic cytoarchitecture (7, 8, 10–12). These changes have been measured in neonatal piglets (13), cats (14), and mice (15), and in pioneering studies of preterm infants (3, 4, 8).

The present study used structural MRI and DTI to examine the spatial and temporal development of human cortical microstructure. We reasoned that if the process was impaired by preterm birth we should observe a dose-dependent reduction in the rates of change of anisotropy and diffusivity, with higher values in preterm infants studied at term (38–42 wk postconception) compared with healthy infants born at term. If this process was developmentally important it should be reflected in neurodevelopmental abilities during later childhood. Further, the tension theory of cortical morphogenesis (16, 17) argues that early maturation of long-distance cortical connectivity establishes cortical sulci with gyri developing later between these fixed points, thus predicting lower diffusivity and anisotropy locally in sulci compared with the gyral crest, and globally in regions of early sulcation. Such differences might reflect local vulnerability.

We tested these predictions in complementary analyses of data obtained from infants imaged between 27 and 46 wk postconception. First, we sampled MD and FA in sulcal and gyral regions of interest (ROIs) in the frontal, parietal, temporal, and occipital cortices, modeling development over time and comparing it to neurodevelopmental abilities at 2 y of age. Second, we developed a nonsubjective, data-driven computational method to extract data from voxels across the whole cortex and to cluster them according to developmental trajectories, providing a global survey of microstructural development with voxel-wise resolution and allowing for comparisons with local growth in cortical surface area.

We now report that MD decreased consistently throughout the study period, but the decline in FA was undetectable after 38 wk postconception, despite not reaching normal levels in preterm infants. Microstructural development followed the pattern predicted by the tension hypothesis, and was altered by preterm birth with slower maturation predicting worse neurodevelopmental function at 2 y of age.

Results

Microstructural Change in Regions of Interest. Fifty-five preterm infants were studied, 11 more than once, providing 66 datasets between 27 and 46 wk postconception. Changes in FA were best modeled by a biphasic piecewise generalized linear regression with a node at 38 wk gestational age (Fig. 1). MD was best modeled by a monophasic generalized linear regression (Fig. 2). These models are given in Table S1.

Before 38 wk, FA fell significantly in all sampled regions, but was higher and fell faster in gyri than sulci (Table S1) and in frontal compared with other regions (Table S2); after 38 wk there were no significant changes (Table S1). In contrast, whereas MD fell in all regions except the frontal sulci, it continued to decline after 38 wk (Table S1). MD was also higher in gyri than sulci, but rate of change did not differ significantly except between frontal and occipital regions (Tables S1 and S2).
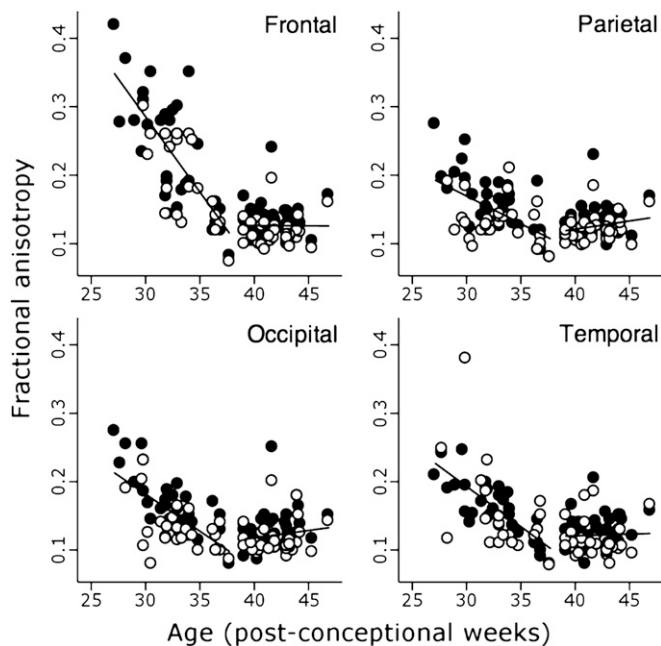
NEUROSCIENCE

Fig. 1. Regional changes in FA. Change in FA in cortical ROIs demonstrated by piecewise linear regression. ROIs were placed in gyri (black circles) and sulci (white circles) of frontal, parietal, occipital, and temporal cortex, and regression lines are shown for all samples. Note that FA is generally higher in the gyri in all four regions.

The decline in FA was reduced by longer exposure to extra-uterine life (Table S1), and FA was significantly higher in the 37 preterm infants imaged at term-corrected age than in 10 infants delivered at term after uncomplicated pregnancies (Fig. 3; $P <$ 0.0001). No dose-dependent effect of prematurity on the rate of change in MD was detected, but MD was also higher in preterm infants at term-corrected age than in term-born infants, although still falling rapidly (Fig. 3; $P < 0.0001$).

In 39 preterm infants for whom the Griffiths' developmental quotient (DQ) was measured at around 2 y of age, higher DQ was related to more rapid changes in FA and in MD during the preterm period; however, after correction for multiple measurements, only the latter remained significant ($P = 0.028$).

Whole-Cortex Survey. Images from 47 of the preterm cohort, including seven infants studied twice, were suitable for analysis using a method to survey changes in MD and FA across the whole cortex: gray matter-based spatial statistics, derived from tract-based spatial statistics (TBSS). Average FA at different ages during the preterm period is shown in Fig. 4A, and 4D maps of FA change over time are presented in Movies S1 and S2. Cortical voxels were grouped according to change in FA over time into three clusters, which provided the optimum representation of the data after repeated iterations of the k-means algorithm. The trajectories of FA change within each of the three clusters are shown in Fig. 4B, together with a randomly chosen set of 100 voxels per cluster to give a representation of the spread of the data. The anatomical locations of the clusters, which showed general but not complete hemispheric homology, are shown in Fig. 4C. In addition to these three clusters, a few voxels (6%) showed increasing FA trajectory, representing misclassified white matter, and were removed from the analysis.

Cortical trajectories of FA reproduced the biphasic pattern seen in the ROI analysis, with the decline in FA before 38 wk gestational age evident in clusters 2 and 3. Cluster 3 had the highest initial FA values and most rapid decrease: voxels with

this time course were found predominantly in the frontal pole; superior and lateral parietal cortex; in the anterior temporal poles bilaterally; and in the left temporoparietal junction. Cluster 2 had a similar time course but with a lower initial FA value, and were widely distributed across lateral frontal, middle temporal, and lateral parietal cortices. FA in cluster 1 changed relatively little across the study period: these voxels were found predominantly in inferior frontal, medial occipital, and perirolandic cortex bilaterally, and right temporal regions.

Cortical MD was best described by a two-cluster model. MD at different ages is shown in Fig. 5A, and maps of MD change over time are presented in Movies S3 and S4. Fig. 5B shows the trajectory centers overlaid on 100 randomly sampled time courses, and cluster location is shown in Fig. 5C. MD decreased globally, with moderately higher values in cluster 1, located in superior, inferior frontal and prefrontal cortex, anterior temporal lobe, insula, and superior parietal cortex.

Localized measures of cortical growth were estimated by calculating the Jacobian determinants of the deformation fields that align the volumetric MR images to a population-based, spatiotemporal brain atlas. Growth varied across the cortex, but the average log-Jacobian in each of the clusters defined by FA trajectory showed a linear relation to the postconceptional age of the infant at imaging (Fig. 6 A–C). The rate of cortical growth was significantly related to the rate of FA change ($P < 0.001$; Fig. 6D).

Discussion

This spatiotemporal mapping of diffusion in human cerebral cortex from 27 to 46 wk postconception offers the opportunity of using millimeter-scale imaging data to infer the development of millimeter-scale neural organization across the whole cortex through reference to neuroanatomical data and diffusion–neuroanatomic correlations. Age-matched human neuroanatomic samples reveal the creation of an increasingly dense and complex cytoarchitecture during this period through dendritic arborization, glial proliferation, differentiation of radial glia, and synapse formation (18–21). Particular studies show that the length of basal dendrites,
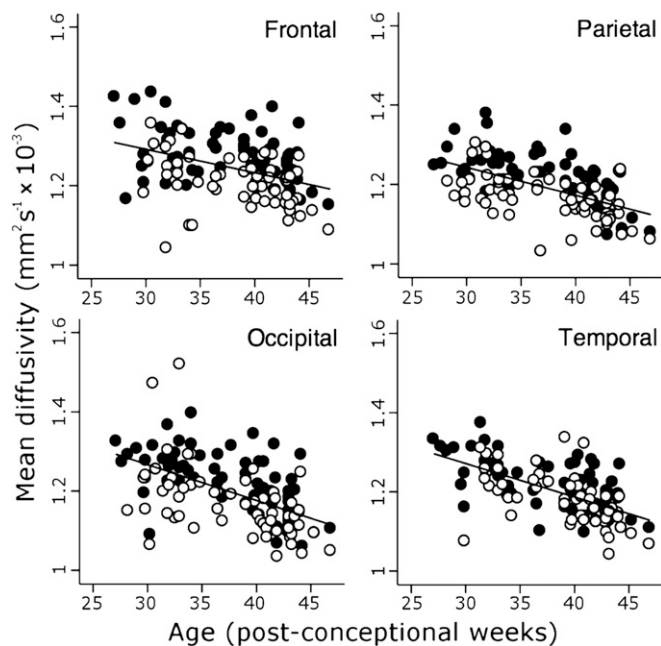

Fig. 2. Regional changes in mean diffusivity. Change in MD in cortical ROIs demonstrated by linear regression. Data labeled as in Fig. 1. Note that MD is generally higher in the gyri in all four regions, and that in contrast to FA, the decline in MD continues after 38 wk of age.
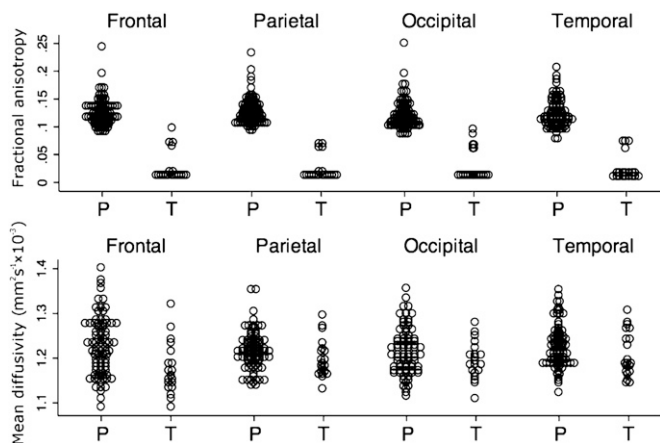
www.manaraa.com

Fig. 3. FA and MD at term-corrected age. FA and MD extracted from cortical ROIs were compared between all preterm infants imaged at term-corrected age (P; *n* = 37) and a cohort of healthy, term-born controls (T; *n* = 10). Cortical FA and MD were both significantly higher in the preterm infants at term in all regions.

dendritic spine density, and synapse number at term are lower in frontal association cortex than in primary sensory or motor regions (22, 23), and that the elongation of dendrites and the order of basal (but not apical) dendritic branching is complete at 38–40 wk postconception (24, 25). Microstructural maturation can also be altered by perinatal stress, which leads to the retraction of apical dendrites (26).

Direct diffusion–neuroanatomic correlations are difficult to acquire in human infants, and the data are few and only partially relevant (27). Fortunately, precise information is available from experimental studies. In developing rodents, the reductions of MD and FA colocalize and correlate with increased dendritic density and fewer nestin-positive radial glia (28); in ferrets, FA is higher in regions with less-differentiated neurons and fewer orthogonal dendrites (29); and in preterm sheep, cerebral ischemia disrupts the normal maturational fall in cortical FA in proportion to a reduction in the complexity of the basal dendritic arbor of pyramidal neurons (30).

Many of the processes underlying mammalian cortical development are preserved across species (19). Though cross-species comparisons require caution, the consistency of the human and experimental data argues strongly that the observed diffusion changes are the consequence of neural growth and differentiation, with decreasing MD reporting growing tissue density secondary to increasing neurite number, cellular complexity, and synapse formation, and the fall in FA predominantly reflecting increasing dendritic elongation and branching orthogonal to cortical columns, particularly in the basal arbor. Other potential changes, such as differentiation of radial glia or retraction of apical dendrites, could also contribute but are likely to be quantitatively less significant.

The current results are thus best understood as showing a consistent increase in cellular and synaptic complexity starting earlier in sulci than gyri, with rapid elongation of dendrites beginning in sulci and regions of early sulcation, then spreading into gyri and higher-order association cortex before slowing markedly after 38 wk postconception.

This complex microstructural development was impaired in a dose-dependent manner by premature exposure to the extra-uterine environment, and at term-corrected age, preterm infants showed significantly higher MD and FA than term-born controls. MD was still falling, consistent with ongoing increases in dendritic spine density and synaptogenesis (22, 31–33), but there was no suggestion of compensatory development in the aspects of dendritic arborization reflected by FA measurements. Gray matter-based spatial statistics may provide an appropriate method for further studies to determine whether differences persist.

The cortex-wide correlations between local developmental trajectories of FA and growth in cortical volume extend previous sample-based analyses and confirm the local synchronization of
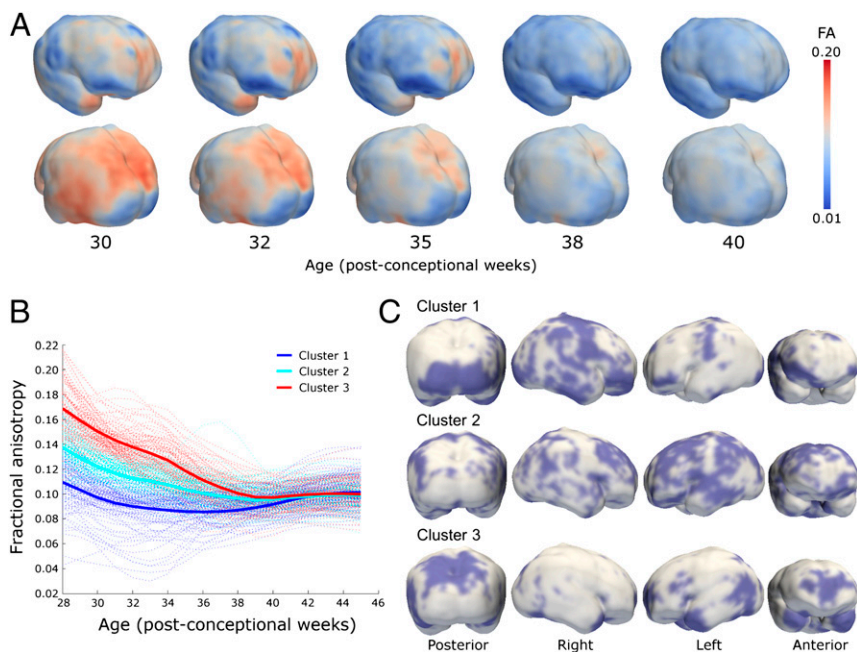

Fig. 4. Global spatiotemporal mapping of changes in FA. (*A*) Cortical FA at five time-points during the preterm period mapped onto a smoothed isosurface representation of the population-based template image. (*B*) Cortical voxels were clustered into three groups according to the trajectory of change in FA over time. Kernel regression shows the developmental trajectory of FA in each cluster (thick solid lines) overlaid on 100 randomly sampled voxel time-courses from within each cluster (thin lines). (*C*) Cluster locations displayed on the same surface as *A*.
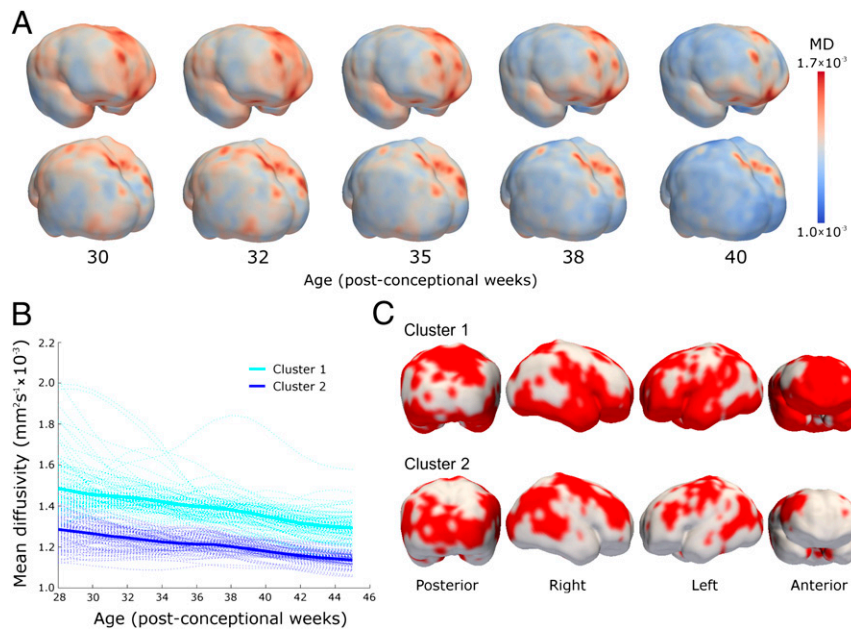
Ball et al.

NEUROSCIENCE

www.manaraa.com

Fig. 5. Global spatiotemporal mapping of changes in MD. (*A*) Cortical MD at five time-points during the preterm period. (*B*) Cortical voxels were clustered into two groups based on the trajectory of MD change over time. Kernel regression shows trajectory of group-average MD in both clusters (thick lines) overlaid onto 100 randomly sampled voxel time courses (thin lines). (*C*) Cluster locations are displayed as in Fig. 4.

microscopic and macroscopic maturation (34). This program may also coordinate with the growth of functional connectivity, because the regions with most rapid development are predominantly higher-order association areas that are engaged by functional networks, such as the executive and default mode systems, which show greater changes than primary auditory or visual networks during this period (35).

Fig. 6. Parallel microstructural development and macrostructural growth in the cortex. The relation between increasing cortical volume, represented by the log-Jacobian determinant, and postconceptional age in voxels clustered by spatiotemporal mapping of cortical FA (*A*, cluster 1; *B*, cluster 2; *C*, cluster 3; location of clusters shown in Fig. 4). Rate of change of volume over time was significantly different in each cluster (*D*).

The rate of cortical growth and maturation was rapid during the studied period, and predicted neurodevelopmental test scores in later childhood (36, 37). Development was most rapid in the frontal pole, which stands at the apex of the prefrontal hierarchy, engaged in goal-setting and monitoring (38); the temporal pole, involved in social and emotional processing (39); and the parietal association cortex, critical for working memory and visual–spatial processing (40). These functions are frequently specifically impaired in children born preterm, consistent with the hypothesis that rapid microstructural growth confers vulnerability to the effect of premature extrauterine life.

These results suggest a mechanism for the reduced cognitive abilities in preterm infants; demonstrate the importance of brain development in the late preterm period; and may help account for the adverse effects of even minor degrees of prematurity (41).

Materials and Methods

Subjects. The study was approved by the Hammersmith Hospital Research Ethics Committee, and infants were recruited after written informed parental consent. Clinical information for the preterm cohort is given in *SI Materials and Methods* and Table S3. No infants had evidence of cystic periventricular leukomalacia or hemorrhagic parenchymal infarction on conventional MRI.

Image Acquisition. Fifteen-direction DTI and T2-weighted MRI was performed on a Philips 3.0 Tesla system using an eight-channel phased-array head coil. MR procedures are described in detail in *SI Materials and Methods*.

ROI Analysis. DTI data were processed using DTI Studio version 2.1 (42). Diffusion tensors were estimated voxel-wise to create FA and MD maps. Multiple ROIs were manually delineated in ~8–10 axial slices of the MD maps, depending on the maturity of the brain. Each slice had 10–20 regions delineated on both cortical gyri and sulci bilaterally of all four cortical lobes: frontal, parietal, occipital, and temporal (Fig. S1).

Investigation of Partial-Volume Effects. To analyze possible partial-volume effects of cerebrospinal fluid on measurements, three infants at 26 wk, 34 wk, and term-equivalent age were subject to an additional diffusion fluid-attenuated inversion recovery, or FLAIR, sequence during the same acquisition. The influence of partial-volume effects on diffusion measures was tested (*SI Materials and Methods*; Fig. S1) and no evidence of significant contamination was found.
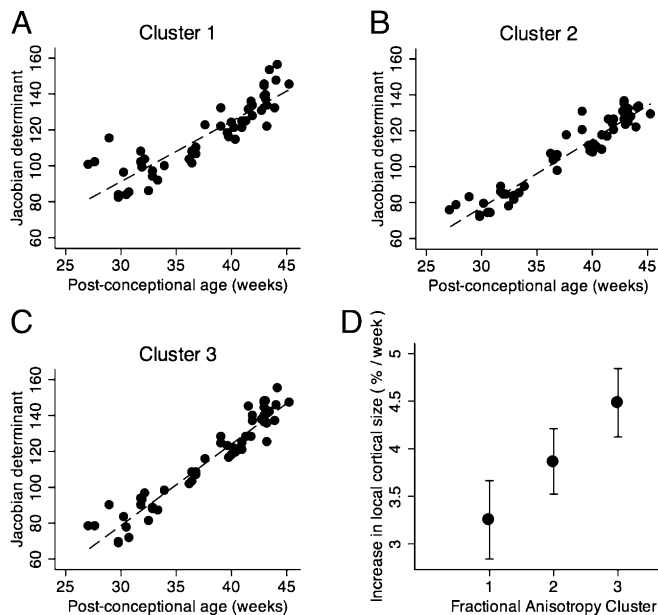
Statistical Modeling. Stata 12.1 (StataCorp) was used for all statistical analyses. To account for repeated sampling in some individuals, we used generalized least-squares regression to create parallel models of the rate of change in FA and MD values. The effects of postconceptional age, length of extrauterine life, brain region, sulcus or gyrus, total brain volume, and their interactions were examined in a series of regression models, and the most informative model chosen using the Akaike and Bayesian information criteria; these included the postconceptional age, brain region, gyrus or sulcus, and length of extrauterine life as main effects alongside the interactions between postconceptional age and the other variables. The selected models were tested by inspecting histograms of idiosyncratic and subject-specific errors and normal quantile (Q–Q) plots; these showed adequate fitting but disclosed outliers that were removed with change to inferences. Stability was analyzed using perturbation analysis, adding random values to variables and reestimating the model 200 times.

Inspection of the raw data showed nonlinear changes in FA over time and we therefore tested models based on first- and second-order polynomials and biphasic linear piecewise regression with a node placed at 38 wk postconception. Both polynomial and piecewise methods produced appropriate models, but perturbation analysis showed relative instability in the polynomial regression, and biphasic piecewise analysis was used for analysis. MD was less obviously biphasic, and information criteria favored the monophasic model, which we report; however, the results for mono- or biphasic regressions were broadly similar, though the differences between gyri and sulci were less, and the effect of prematurity more, significant in the biphasic analysis. Post hoc Wald tests were used to determine where significant differences existed between rate of change in each brain region and across time periods (pre- and post-38 wk).

To confirm the effect of prematurity, we compared preterm infants imaged at term-corrected age with 10 term-born control subjects using analysis of variance, with age at scan, brain region, gyrus or sulcus, and subject group (preterm/control) as main effects.

Neurodevelopmental Outcome. Infants in the study were offered entry into a follow-up program. At ~2 y corrected age, 39 subjects undertook the Griffith Mental Developmental Scales, which provide an overall DQ made up of locomotor; personal and social; hearing and language; eye–hand coordination; and performance subscales. The relation of DQ to changes in FA and MD were tested, and the contributions of the component subscales explored by linear regression. To aid interpretation of main effects, data were demeaned and models were corrected for multiple measurements from each individual.

Voxel-Wise Analysis. Fifty-four images were included for voxel-wise analysis after ensuring both that T2-weighted structural MRI and DTI were free from artifacts that would preclude computational processing and alignment to the template space of all images was accurate. The subset did not significantly differ from the full cohort in age at birth or at imaging.

Image Processing. We describe a unique method for aligning cortical data from multiple subjects into a common space to provide a voxel-wise spatial characterization of FA and MD change across the whole cortex.

To resolve regional differences in cortical anisotropy, it is necessary to align anatomically correspondent regions across individuals. To mitigate the confounding effects of anatomical misalignment between subjects and to remove partial-volume contamination due to the arbitrary choice of smoothing kernel often used in such analyses, we adapt a well-known processing pipeline for diffusion data designed to overcome such issues, TBSS (43), to generate gray matter-based spatial statistics for use in cortical analysis.

Image processing was performed with FSL (version 4.1.9) (44), and the processing pipeline is illustrated in Fig. S2. Diffusion datasets were corrected for distortion due to eddy currents, and FA and MD maps were constructed. Nonlinear registration (using the IRTK software package, www.doc.ic.ac.uk/~dr/software/) (45) was used to align each infant's non–diffusion-weighted ($b = 0$) image to their corresponding T2-weighted structural image. T2 volumes were bias corrected and segmented into three tissue classes (cortex, white matter, cerebrospinal fluid) using FAST ("FMRIB's Automated Segmentation Tool," Functional MRI of the Brain Centre, Oxford, UK) and age-appropriate anatomical priors (46). Nonlinear image registration was used to align each T2 image to a population-based template at a time-point close to the mean age of the group at the time of imaging (gestational week 36). Registration was performed in two steps, first to an age-appropriate T2 template within a population-based, spatiotemporal atlas (46), followed by longitudinal

registration toward to the final 36-wk template (47). Probabilistic cortical tissue maps were inspected and transformed to the common template space alongside FA and MD maps (via the intermediate T2 image).

A mean cortical map was produced by merging the aligned cortical probability maps, and skeletonized to retain only a core of highly probable cortical voxels as a thin curved surface at the center of the cortex. Individual cortical measurements were then projected onto the cortical skeleton; this was achieved by searching in a direction perpendicular to the cortical skeleton identifying maximally probable cortical voxels in each of the spatially transformed cortical probability maps, such that only data from nearby voxels with maximal cortical probability were kept and projected onto the skeleton. FA and MD data from the identified cortical voxels were then projected onto the skeleton for analysis. In contrast to TBSS, data projection was based not on aligning voxels with high FA, because FA was expected to vary dramatically across the cohort. Instead, voxels with high probability of containing gray matter were sought, thus ensuring that only diffusion measures from cortical voxels were analyzed. To further remove the possibility of analyzing voxels that did not contain FA data due to misregistration of individual subjects' diffusion and T2 images, voxels with a mean value across the whole group of less than 0.005 were excluded from the analysis.

Spatial Characterization of Microstructural Change. Skeletonized cortical voxels were grouped according to the trajectory of change in FA and MD across the cohort using a combination of kernel regression and unsupervised clustering.

Because the ages of the subjects were irregularly scattered over the time interval studied, kernel regression was applied to generate, for each voxel, group average measurements of FA at a regular sequence of time points.

Let y_{is} denote the measurement at voxel i for subject s; let a_s represent the age of subject s. The kernel regression estimate for the value at age (time) t for voxel i is given by

$$y_i(t) = \frac{1}{z} \sum_s y_{is} \, \exp\left(-(t - a_s)^2 / \kappa^2\right).$$

The width parameter, κ, was chosen so that the kernel's full width at half-maximum was 4 wk, and z is a normalizing constant. A sequence of regularly spaced ages (values of t) at 1-wk intervals over the age range is denoted by $\{t_k\}$ for $k = 1, \ldots, K$ and the vector $\mathbf{y}_i = (y_{i1}, \ldots, y_{iK})^T$ represents the measurements at voxel i for the regular time points $\{t_k\}$.

The set of all time-regularized vectors $\{\mathbf{y}_i\}$ for $i = 1, \ldots, N$, where N is the total number of voxels, was grouped into clusters using k-means; this provides C cluster centroids $\mu_1, \ldots, \mu_C$ such that each voxel is assigned to the cluster with the nearest Euclidean distance, i.e., the cluster label assigned to voxel i is z_i, $1 \le z_i \le C$, where $z_i = \arg \min_z (\mathbf{y}_i - \mu_z)^2$. The k-means algorithm is an iterative stochastic method that is initialized with randomized estimates for the trajectory centers and is run to convergence multiple times. Ten repeated starts were used with the initial estimates derived from a random subsample of 10% of the voxels. The whole process was repeated, varying numbers of clusters, and the final number of clusters for each type of data was selected to be the largest for which no empty clusters were generated during the iterations of the algorithm.

Macrostructural Development over Time. Using the method described above, maps of relative volume change were calculated in the form of the Jacobian determinant of the transformation aligning each T2 image to the population-based template image. These values were projected onto the mean cortical skeleton from high-probability cortical voxels in an analysis analogous to deformation (or tensor)-based morphometry (45, 48). Logarithms of voxel-wise Jacobian values were calculated, averaged over every voxel within a cluster, and the rate of change of volume over the age interval compared between clusters with multivariate regression. Outliers were assessed by inspection of Cook's distance, and dropped if the value was greater than 0.2. A post hoc Wald test was used to test for differences between slopes.

1. Bystron I, Blakemore C, Rakic P (2008) Development of the human cerebral cortex: Boulder Committee revisited. *Nat Rev Neurosci* 9(2):110–122.

2. Le Bihan D (1995) Molecular diffusion, tissue microdynamics and microstructure. *NMR Biomed* 8(7-8):375–386.

Ball et al.

NEUROSCIENCE

3. Neil JJ, et al. (1998) Normal brain in human newborns: Apparent diffusion coefficient and diffusion anisotropy measured by using diffusion tensor MR imaging. *Radiology* 209(1):57–66.

4. Mukherjee P, et al. (2002) Diffusion-tensor MR imaging of gray and white matter development during normal human brain maturation. *AJNR Am J Neuroradiol* 23(9):1445–1456.

5. Gupta RK, et al. (2005) Diffusion tensor imaging of the developing human cerebrum. *J Neurosci Res* 81(2):172–178.

6. Dobbing J, Sands J (1973) Quantitative growth and development of human brain. *Arch Dis Child* 48(10):757–767.

7. Takashima S, Chan F, Becker LE, Armstrong DL (1980) Morphology of the developing visual cortex of the human infant: A quantitative and qualitative Golgi study. *J Neuropathol Exp Neurol* 39(4):487–501.

8. McKinstry RC, et al. (2002) Radial organization of developing preterm human cerebral cortex revealed by non-invasive water diffusion anisotropy MRI. *Cereb Cortex* 12(12):1237–1243.

9. Samuelsen GB, et al. (2003) The changing number of cells in the human fetal forebrain and its subdivisions: A stereological analysis. *Cereb Cortex* 13(2):115–122.

10. Lund JS, Boothe RG, Lund RD (1977) Development of neurons in the visual cortex (area 17) of the monkey (*Macaca nemestrina*): A Golgi study from fetal day 127 to postnatal maturity. *J Comp Neurol* 176(2):149–188.

11. Petit TL, LeBoutillier JC, Gregorio A, Libstug H (1988) The pattern of dendritic development in the cerebral cortex of the rat. *Brain Res* 469(1-2):209–219.

12. Jespersen SN, Leigland LA, Cornea A, Kroenke CD (2012) Determination of axonal and dendritic orientation distributions within the developing cerebral cortex by diffusion tensor imaging. *IEEE Trans Med Imaging* 31(1):16–32.

13. Thornton JS, et al. (1997) Anisotropic water diffusion in white and gray matter of the neonatal piglet brain before and after transient hypoxia-ischaemia. *Magn Reson Imaging* 15(4):433–440.

14. Baratti C, Barnett AS, Pierpaoli C (1999) Comparative MR imaging study of brain maturation in kittens with T1, T2, and the trace of the diffusion tensor. *Radiology* 210(1):133–142.

15. Zhang J, et al. (2006) Characterization of mouse brain and its development using diffusion tensor imaging and computational techniques. *Conf Proc IEEE Eng Med Biol Soc* 1:2252–2255.

16. Van Essen DC (1997) A tension-based theory of morphogenesis and compact wiring in the central nervous system. *Nature* 385(6614):313–318.

17. Hilgetag CC, Barbas H (2005) Developmental mechanics of the primate cerebral cortex. *Anat Embryol (Berl)* 210(5-6):411–417.

18. Mrzljak L, Uylings HBM, Kostovic I, Van Eden CG (1988) Prenatal development of neurons in the human prefrontal cortex: I. A qualitative Golgi study. *J Comp Neurol* 271(3):355–386.

19. Marín-Padilla M (1992) Ontogenesis of the pyramidal cell of the mammalian neocortex and developmental cytoarchitectonics: A unifying theory. *J Comp Neurol* 321(2):223–240.

20. Prinz M, Prinz B, Schulz E (1997) The growth of non-pyramidal neurons in the primary motor cortex of man: A Golgi study. *Histol Histopathol* 12(4):895–900.

21. Rakic P (2003) Developmental and evolutionary adaptations of cortical radial glia. *Cereb Cortex* 13(6):541–549.

22. Huttenlocher PR, Dabholkar AS (1997) Regional differences in synaptogenesis in human cerebral cortex. *J Comp Neurol* 387(2):167–178.

23. Travis K, Ford K, Jacobs B (2005) Regional dendritic variation in neonatal human cortex: A quantitative Golgi study. *Dev Neurosci* 27(5):277–287.

24. Becker LE, Armstrong DL, Chan F, Wood MM (1984) Dendritic development in human occipital cortical neurons. *Brain Res* 315(1):117–124.

25. Lu D, et al. (2013) Somal and dendritic development of human CA3 pyramidal neurons from midgestation to middle childhood: A quantitative Golgi study. *Anat Rec (Hoboken)* 296(1):123–132.

26. Murmu MS, et al. (2006) Changes of spine density and dendritic complexity in the prefrontal cortex in offspring of mothers exposed to stress during pregnancy. *Eur J Neurosci* 24(5):1477–1487.

27. Trivedi R, et al. (2009) Region-specific maturation of cerebral cortex in human fetal brain: Diffusion tensor imaging and histology. *Neuroradiology* 51(9):567–576.

28. Sizonenko SV, et al. (2007) Developmental changes and injury induced disruption of the radial organization of the cortex in the immature rat brain revealed by in vivo diffusion tensor MRI. *Cereb Cortex* 17(11):2609–2617.

29. Bock AS, et al. (2010) Diffusion tensor imaging detects early cerebral cortex abnormalities in neuronal architecture induced by bilateral neonatal enucleation: An experimental model in the ferret. *Front Syst Neurosci* 4:149.

30. Dean JM, et al. (2013) Prenatal cerebral ischemia disrupts MRI-defined cortical microstructure through disturbances in neuronal arborization. *Sci Transl Med* 5(168):168ra7.

31. Marin-Padilla M (1967) Number and distribution of the apical dendritic spines of the layer V pyramidal cells in man. *J Comp Neurol* 131(4):475–490.

32. Glantz LA, Gilmore JH, Hamer RM, Lieberman JA, Jarskog LF (2007) Synaptophysin and postsynaptic density protein 95 in the human prefrontal cortex from mid-gestation into early adulthood. *Neuroscience* 149(3):582–591.

33. Webster MJ, Elashoff M, Weickert CS (2011) Molecular evidence that cortical synaptic growth predominates during the first decade of life in humans. *Int J Dev Neurosci* 29(3):225–236.

34. Deipolyi AR, et al. (2005) Comparing microstructural and macrostructural development of the cerebral cortex in premature newborns: Diffusion tensor imaging versus cortical gyration. *Neuroimage* 27(3):579–586.

35. Doria V, et al. (2010) Emergence of resting state networks in the preterm human brain. *Proc Natl Acad Sci USA* 107(46):20015–20020.

36. Kapellou O, et al. (2006) Abnormal cortical development after premature birth shown by altered allometric scaling of brain growth. *PLoS Med* 3(8):e265.

37. Rathbone R, et al. (2011) Perinatal cortical growth and childhood neurocognitive abilities. *Neurology* 77(16):1510–1517.

38. Tsujimoto S, Genovesio A, Wise SP (2011) Frontal pole cortex: Encoding ends at the end of the endbrain. *Trends Cogn Sci* 15(4):169–176.

39. Olson IR, Plotzker A, Ezzyat Y (2007) The enigmatic temporal pole: A review of findings on social and emotional processing. *Brain* 130(Pt 7):1718–1731.

40. Koenigs M, Barbey AK, Postle BR, Grafman J (2009) Superior parietal cortex is critical for the manipulation of information in working memory. *J Neurosci* 29(47):14980–14986.

41. Quigley MA, et al. (2012) Early term and late preterm birth are associated with poorer school performance at age 5 years: A cohort study. *Arch Dis Child Fetal Neonatal Ed* 97(3):F167–F173.

42. Jiang H, van Zijl PCM, Kim J, Pearlson GD, Mori S (2006) DTIStudio: Resource program for diffusion tensor computation and fiber bundle tracking. *Comput Methods Programs Biomed* 81(2):106–116.

43. Smith SM, et al. (2006) Tract-based spatial statistics: Voxelwise analysis of multi-subject diffusion data. *Neuroimage* 31(4):1487–1505.

44. Smith SM, et al. (2004) Advances in functional and structural MR image analysis and implementation as FSL. *Neuroimage* 23(Suppl 1):S208–S219.

45. Rueckert D, Frangi AF, Schnabel JA (2003) Automatic construction of 3-D statistical deformation models of the brain using nonrigid registration. *IEEE Trans Med Imaging* 22(8):1014–1025.

46. Serag A, et al. (2012) Construction of a consistent high-definition spatio-temporal atlas of the developing brain using adaptive kernel regression. *Neuroimage* 59(3):2255–2265.

47. Serag A, et al. (2012) LISA: Longitudinal image registration via spatio-temporal atlases. *The 2012 9th IEEE International Symposium on Biomedical Imaging (ISBI)*, 10.1109/ISBI.2012.6235552.

48. Ashburner J, et al. (1998) Identifying global anatomical differences: Deformation-based morphometry. *Hum Brain Mapp* 6(5-6):348–357.

www.manaraa.com